Single-image Background Removal with Entropy Filtering

Chang-Chieh Cheng[a]

Information Technology Service Center, National Chiao Tung University, 1001 University Road, Hsinchu, Taiwan

Keywords: Background Removal, Segmentation, Entropy, Texture Analysis.

Abstract: Background removal is often used for segmentation of the main subject from a photograph. This paper proposes a new method of background removal for a single image. The proposed method uses Shannon entropy to quantify the texture complexity of background and foreground areas. A normalized entropy filter is applied to compute the entropy of each pixel. The pixels can be classified effectively if the entropy distributions of the background and foreground can be distinguished. To optimize performance, the proposed method constructs an image pyramid such that most background pixels can be labeled in a low-resolution image; thus, the computational cost of entropy calculation can be reduced in the image with the original resolution. Connected component labeling is also adopted for denoising to retain the main subject area completely.

1 INTRODUCTION

Background removal is a digital image processing procedure that can be used to classify parts of an image in terms of unwanted and interest regions. Many applications of image processing and computer vision require background removal before further analysis and processing. For example, object segmentation within a single photograph requires background removal (Chen et al., 2016). Background removal also can be applied to a series of images including videos and images taken from different views. For example, background removal can be applied for foreground object extraction from videos (Kumar and Yadav, 2016) and 3D object reconstruction from multiview images (Gordon et al., 1999)(Tsai et al., 2007). Since multiple images can provide more information regarding backgrounds than a single image can, removing backgrounds from multiple images may be more accurate than removing a single background from a single image.

This paper proposes a method of background removal for a single image (BRSI). The fundamental method of BRSI is the intensity-based region method (IBR), which classifies pixels according to their background and foreground intensities. One commonly used IBR method is the thresholding-based (TB) method, which uses a specified intensity value as a threshold and classifies pixels as background if their intensities are less than the threshold (Gonzalez and Woods, 2006). The TB method can be improved by histogram-based (HB) background removal (Gonzalez and Woods, 2006), which constructs an intensity histogram from an image to find the intensity range of the background with the maximum bin count of the histogram. Therefore, the pixels belong to the background if their intensity values are in the specified intensity range. Although the implementation of IBR is easy, misclassification occurs if the intensity distribution of the background is so wide that deciding the threshold and intensity range of background is difficult. Nevertheless, the HB method can be improved by intensity clustering. K-means clustering (Zhang and Luo, 2012) and Gaussian mixture models (GMMs) (Huang and Liu, 2007) are commonly used methods for finding K clusters from a set of data. Therefore, the intensities in an image can be divided into several groups by using K-means or GMMs. The background intensity value is decided by the mean of the most common group. However, clustering may fail if the intensities of background are distributed over a wide range.

In recent years, many machine learning techniques, such as the support vector machine (Wang et al., 2011) and random forest (Schroff et al., 2008), have been used for BRSI. A convolutional neural network (CNN), which is an artificial neural network with multiple convolution layers, can be used for segmentation of interesting regions from an image (Ronneberger et al., 2015). However, for high-accuracy classification, most methods of machine learning re-

[a] https://orcid.org/0000-0002-9103-3400

Cheng, C.
Single-image Background Removal with Entropy Filtering.
DOI: 10.5220/0010301204310438
In *Proceedings of the 16th International Joint Conference on Computer Vision, Imaging and Computer Graphics Theory and Applications (VISIGRAPP 2021) - Volume 4: VISAPP*, pages 431-438
ISBN: 978-989-758-488-6

quire large training sets and incur expensive computational costs in the training phase.

Texture-based segmentation (TEX), a popular method of images segmentation, segments an image into several areas with different degrees of texture. However, TEX requires an appropriate texture analysis. A commonly used method of texture analysis is histogram-based texture analysis (HTA), which creates a histogram to describe the texture around each pixel. One simple HTA method evaluates the probability of occurrence of each intensity (Junqing Chen et al., 2005). Texon is an efficient method of HTA that creates a histogram of oriented gradients (HOG) to describe the orientation and complexity of the region around a pixel (Malik et al., 2001). In information theory, Shannon entropy (Shannon, 2001) is often used to evaluate the complexity of a data set. Several studies have reported that the Shannon entropy can be used for image segmentation (Zhang et al., 2003)(Qi, 2014).

This paper proposes an efficient approach to BRSI based on TEX with Shannon entropy to classify foreground and background areas that have different complexities of texture. The proposed approach uses the pyramid method (Adelson et al., 1983) to evaluate the texture complexity in a multiscale representation of the input image. Connected component labeling (CCL) (He et al., 2017) is then applied to eliminate the noisy areas that consist of small fragments and holes. The following statements briefly describe the proposed approach: First, an image pyramid structure is created to represent the input image with different levels of detail. A filter of normalized Shannon entropy is then used to analyze the complexity of pixels from the lowest level, that is, the top of pyramid. During texture analysis, each pixel is classified as background if its entropy is less than a given threshold. Therefore, the pixels in the higher level can be classified as background without the texture analysis only if they can be covered by the background pixels in the lower level. In the other words, pixels only require texture analysis if they are covered by nonbackground pixels of the lower level. After the pixel classification of each layer, CCL then is applied to eliminate the noisy areas.

The remainder of this paper is organized as follows. The Methods section presents the details of the proposed method, including filtering using normalized Shannon entropy, texture analysis in the image pyramid, and background classification. The Results section presents the experimental results from testing on three colorful photographs. Finally, the Discussion section presents a summary and discussion.

2 METHOD

The proposed BRSI method consists of four procedures: entropy filtering, background mapping, image pyramid construction, and denoising. They are respectively detailed in the following four subsections.

2.1 Entropy Filtering

Given an image $I(x,y)$ comprising $M \times N$ pixels, where $x \in \{1,2,\ldots,M\}$ and $y \in \{1,2,\ldots,N\}$, if the values of all pixels of I are categorized into B intensities (i.e. $I(x,y) \in \{t_1,t_2,\ldots,t_B\}$ for all x and y), the Shannon entropy, H, is defined as follows:

$$H(I) = -\sum_{i=1}^{B} P(t_i)\log_{\beta} P(t_i), \tag{1}$$

where $P(t_i)$ is the probability of t_i occurring in I. H is zero if all pixels of I are of a single intensity; otherwise, $H > 0$. Notice that H is maximized if $P(t_i) = \frac{1}{B}, \forall i$; that is,

$$\begin{aligned} \max H(I) &= -\sum_{i=1}^{B} \frac{1}{B}\log_{\beta}\frac{1}{B} \\ &= -B(B^{-1}\log_{\beta} B^{-1}) \\ &= \log_{\beta} B. \end{aligned}$$

If $\beta = B$, H then can be normalized to [0, 1]. Let $\hat{H}$ be the normalized Shannon entropy defined as follows:

$$\hat{H}(I) = -\sum_{i=1}^{B} P(t_i)\log_{B} P(t_i), \tag{2}$$

where $0 \le \hat{H} \le 1$; $\hat{H}$ can then be used as a normalized kernel for image filtering. Given a window with $\hat{M}$ columns and $\hat{N}$ rows, the equation of filtering with I can be written as follows:

$$\hat{I}(x,y) = \hat{H}(C(I,x,y)), \tag{3}$$

where $\hat{I}$ is the filtered image of I and C crops a subimage of $\hat{M} \times \hat{N}$ pixels around $I(x,y)$. Notice that if B is specified as a large number, the filtering may be sensitive to noise (Knuth, 2006)(Purwani et al., 2017). However, a small value of B may cause the loss of certain significant details. This paper suggests that B can be set as an integer between 16 and 64.

2.2 Background Mapping

The values of $\hat{I}$ can be separated by a threshold τ, where $0 \le \tau \le 1$. Therefore, the pixel at (x,y) is classified as background if $\hat{I}(x,y) < \tau$; otherwise, the pixel

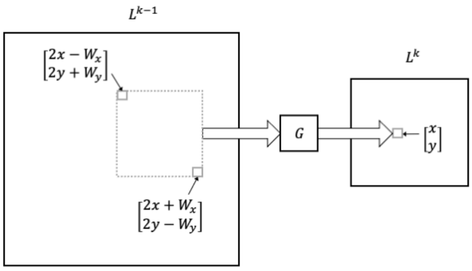
L^{k-1}
$\begin{bmatrix}2x - W_x\\2y + W_y\end{bmatrix}$
$\begin{bmatrix}2x + W_x\\2y - W_y\end{bmatrix}$
G
L^k
$\begin{bmatrix}x\\y\end{bmatrix}$

Figure 1: Constructing L^k.

is classified as foreground. Then, we can create a binary mapping table, T, to categorize each pixel.

$$T(x,y) \quad = \quad \begin{cases} 0 & \text{if } \hat{I}(x,y) < \tau; \\ 1 & \text{otherwise.} \end{cases} \tag{4}$$

However, creating T requires the calculation of $\hat{I}$, as in Eq. (3), which may require excessive computation time if the size of I is large. Let I' be the half-size image of I. Assuming that I' has similar textures to I, the calculation of texture complexity around a pixel $I(x,y)$ can be approximately ignored if $I(x,y)$ is covered by the pixels of I' with texture complexities lower than τ. We then can construct an image pyramid comprising several image layers to express I at different resolutions. Therefore, T can be efficiently determined from the top layer (lowest resolution) to the bottom layer (highest resolution). The following subsection describes the acceleration of T estimation by constructing an image pyramid.

2.3 Image Pyramid Construction

An image pyramid L of K layers constructed from I can be expressed as Fig. 1, where $k = \{1,2,\ldots,K\}$, $x \in \{1,2,\ldots,\lfloor 2^{-(k-1)}M \rfloor\}$, $y \in \{1,2,\ldots,\lfloor 2^{-(k-1)}N \rfloor\}$, $L^1 = I$, and G is a low-pass filter of size $(2W_x+1)\times(2W_y+1)$ pixels, for example, a 5×5 Gaussian filter. Feature enhancement processing can be applied to I before the construction of the pyramid, for example, such as the Sobel operator for edge detection. Notably, K can be regarded as the number of downsampling iterations. However, information may be lost if excessive downsampling is performed, that is, if K is large. This paper decides K according to the following condition:

$$K \leq \log_2 \frac{\min(M,N)}{N_s}, \tag{5}$$

where N_s is a given constant to represent the minimum size of downsampling. Typically, N_s is specified as 128 or 64.

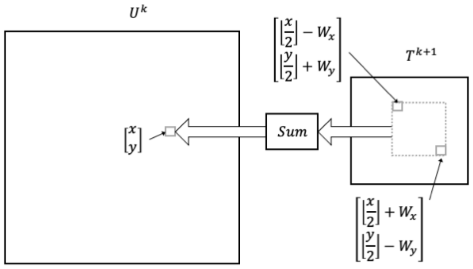
U^k
$\begin{bmatrix}x\\y\end{bmatrix}$
Sum
$\begin{bmatrix}\lfloor\frac{x}{2}\rfloor - W_x\\\lfloor\frac{y}{2}\rfloor + W_y\end{bmatrix}$
T^{k+1}
$\begin{bmatrix}\lfloor\frac{x}{2}\rfloor + W_x\\\lfloor\frac{y}{2}\rfloor - W_y\end{bmatrix}$

Figure 2: Constructing U^k.

We then can apply the entropy filter to L by the following equation:

$$\hat{L}^k(x,y) \quad = \quad \begin{cases} \hat{H}(C(L^k,x,y)) & \text{if } U^k(x,y) \geq \lambda \\ & \text{or } k = K; \\ 0 & \text{otherwise,} \end{cases} \tag{6}$$

where constructing $U^k(x,y)$ is shown in Fig. 2 and

$$T^k(x,y) \quad = \quad \begin{cases} 0 & \text{if } \hat{L}^k(x,y) < \tau; \\ 1 & \text{otherwise.} \end{cases} \tag{7}$$

Notice that $U^k(x,y)$ represents the number of corresponding foreground pixels of (x,y) in layer $k+1$. According to Eq. 6, only the top layer, that is, $k = K$, requires that $\hat{H}$ be applied to all pixels. In the other layers, that is, $k < K$, the calculation of entropy, $\hat{H}(C(L^k,x,y))$, depends on whether $U^k(x,y)$ is larger than a given constant λ. In other words, pixel (x,y) of layer k can be classified as background without a calculation of entropy if $U^k(x,y) < \lambda$. Therefore, the background mapping table of the bottom layer, $T^1(x,y)$, does not require the calculation of$\hat{H}$ for all pixels and the construction of the masking table can be accelerated, especially when the background area is larger than the foreground area.

2.4 Denoising

We now have a binary mapping table to classify each pixel of I as background or foreground. However, many small fragments and holes may be generated in the foreground and background. To address this problem, we use CCL to label each set of adjacent pixels with the same value in a binary image. Given two constants, α_f and α_h , for the area thresholds of fragments and holes, respectively, let $Q(T,\alpha_f,\alpha_h)$ be the CCL function and

$$(\mathbf{A}_f,\mathbf{A}_h) = Q(T,\alpha_f,\alpha_h), \tag{8}$$

where $\mathbf{A}_f = \{\mathbf{a}_f | \mathbf{a}_f$ is a set of adjacent foreground pixels and $|\mathbf{a}_f| \leq \alpha_f$; and $\mathbf{A}_h = \{\mathbf{a}_h | \mathbf{a}_h$ is a set of adjacent background pixels and $|\mathbf{a}_h| \leq \alpha_h\}$. Therefore,

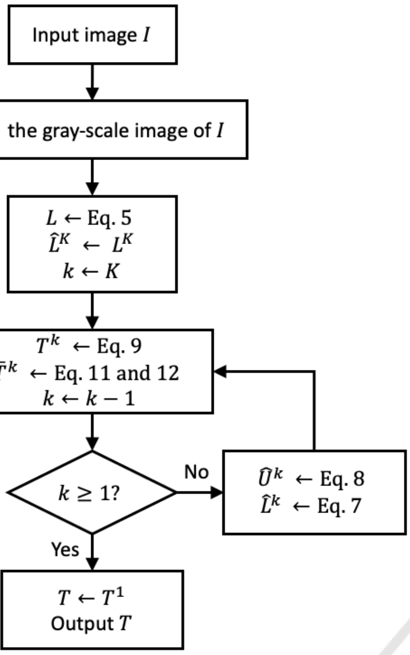

Figure 3: Flowchart of the proposed method.

we can replace T^k with $\bar{T}^k$, which is calculated as follows.

$$\bar{T}^k(x,y) \quad = \quad \begin{cases} 0 & (x,y) \in \mathbf{a}_f^k \subset \mathbf{A}_f^k; \\ 1 & (x,y) \in \mathbf{a}_h^k \subset \mathbf{A}_h^k; \\ T^k(x,y) & \text{otherwise.,} \end{cases} \quad (9)$$

where $k < K$ and

$$(\mathbf{A}_f^k, \mathbf{A}_h^k) = Q(T^k, \alpha_f, \alpha_h). \quad (10)$$

Notice that the computation cost of Q, which includes time and memory consumption, may be high if the image is large. However, many improvement methods have been proposed to address this problem; for example, the two-scan approach to label an $N \times N$ image with complexity $O(N^2)$ (He et al., 2009), and using parallel computing hardware to accelerate labeling (Soman et al., 2010).

The values of α_f and α_h can be determined based on the image size. The experiments described in the next section indicate that the value of α_f ranges from 1% to 10% of the image size, and the value α_h ranges from 10% to 20% of the image size.

Finally, the proposed method is summarized as a flowchart as shown in Fig. 3. The parameters are suggested as follows: $B = 64, \hat{M} = 5, \hat{N} = 5, 0.2 \leq \tau \leq 0.3, K = 3, W_x = 1, W_y = 1, \lambda = 5, \alpha_f = 0.05$, and $\alpha_h = 0.2$.

3 RESULTS

The proposed method was implemented in C++ using the Qt library. The executable file is named EBR and can be downloaded from https://people.cs.nctu.edu.tw/~chengchc/ebr/. EBR was validated by numerous images. This section describes three tests with three different themes images, which were Girl (USC-SIPI,), Birds (Kodak,), and Lighthouse(Kodak,), as shown in Fig. 4. Each test image has at least one foreground subject. The test results demonstrated that these foreground subjects could be segmented with few errors by EBR. The test machine consisted of an Intel i7-7700 CPU and 32GB RAM. The test platform was Windows 10 64-bit.

The first test image was Girl with size 256 × 256 pixels. The foreground is a half-length image of a girl. The test involved manually creating a binary mapping image denoted by T_{g1} to be the ground truth, as shown in Fig. 5e. In the mapping image, the intensities of 1 (white) and 0 (black) represent the foreground and background respectively. Fig. 5a shows the result of removing the background from Fig. 5e. This test also used the HB method to remove the background of Girl, as shown in Fig. 5b and Fig. 5f; Fig. 5f is the mapping image denoted by T_{h1}. EBR then was used for Girl. Fig. 5c and 5g show the results of background removal and the mapping image (T_{n1}) generated by EBR without denoising, respectively, where $B = 64$, $\hat{M} = 3$, $\hat{N} = 3$, $\tau = 0.25$, $K = 3$, $W_x = 1$, $W_y = 1$, and $\lambda = 5$. Notice that the 3×3 Gaussian filtering with a standard deviation of 1.0 and Sobel edge detection were used before the proposed method was applied. However, many obvious fragments and holes appeared in the results. Therefore, EBR was executed with $\alpha_f = 0.05$ and $\alpha_h = 0.2$ for denoising. The execution time was 0.167 s. Fig. 5d and 5h show the result and the mapping image, T_{e1},respectively. For comparison of EBR with the ground truth and HB method, mean square error (MSE) was calculated as follows.

$$MSE(T_a, T_b) = \frac{1}{MN} \sum_{y=1}^{N} \sum_{x=1}^{M} (T_a(x,y) - T_b(x,y))^2. \quad (11)$$

Because T is a binary mapping image, meaning that the value of any pixel in T is either 0 or 1, MSE is an appropriate measurement of error. $MSE(T_{h1}, T_{g1})$, $MSE(T_{n1}, T_{g1})$, and $MSE(T_{e1}, T_{g1})$ were 0.124, 0.167, and 0.015, respectively. For Girl, the error rates of HB and the proposed method were 12.4% and 1.5%, respectively.

Fig. 6 shows the process of EBR at each level. The images in the top row of Fig. 6, which are 6a, 6b, and 6c, show $\hat{L}^3$, $\hat{L}^2$, and $\hat{L}^1$ (Eq. 6), respectively. In

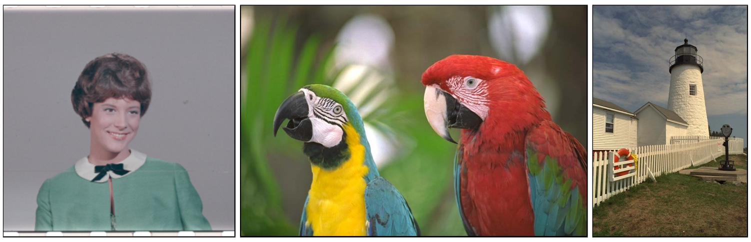

(a) (b) (c)

Figure 4: Test images: (a) Girl, (b) Birds, , and (c) Lighthouse.

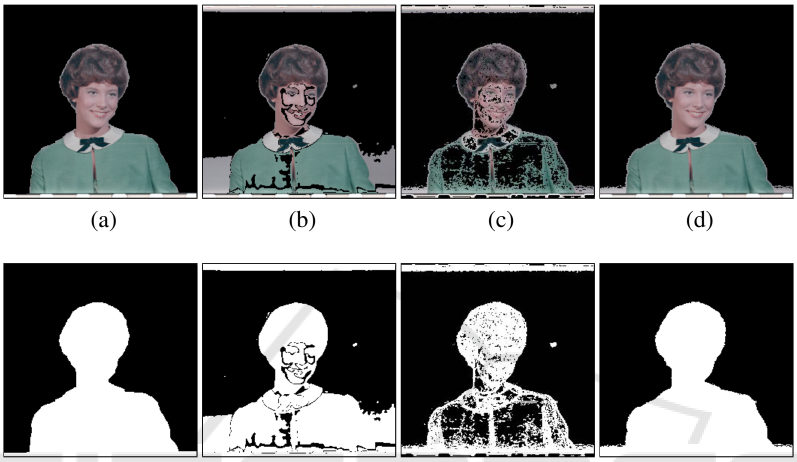

(a) (b) (c) (d)

(e) (f) (g) (h)

Figure 5: Results of Girl. (a) Ground truth. (b) Result of the HB method. (c) Result of EBR without denoising. (d) Result of EBR with denoising. (e),(f),(g),(h) Mapping images of (a),(b),(c),(d), respectively.

each level, the areas of head, body, and outline contain the pixels with high entropy. However, the entropies of the background pixels are near 0. Therefore, the threshold of entropy, τ, can be a small value (approximately 0.25). Fig. 6d, 6e, and 6f show the mapping images without denoising, which are T^3, T^2, and T^1 (Eq. 7), respectively. The denoised mapping images, $\bar{T}^3$, $\bar{T}^2$, and $\bar{T}^1$ (Eq. 9), are shown in Fig. 6g, 6h, and 6i, respectively. As shown in Fig. 6d, the sizes of the noise areas in T^3 are small, approximately 1 to 30 pixels. These noise of T^2 and T^1 are nearly covered by the noise of T^3, and EBR could massively reduce the noise in T^3. Therefore, the computational cost of denoising T^2 and T^1 could also be reduced.

The second test image, Birds, is a colorful photograph measuring 768 × 512 pixels. The foreground objects of Birds are two parrots. Fig. 7a and 7e show the results of manual background removal and its mapping image (T_{g2}), respectively. Because the background of Birds has a wide intensity range, removing the background through the HB method is difficult, as shown in Fig. 7b. The mapping image (T_{h2}) generated by the HB method is shown in Fig. 7f. Next, EBR was applied to Birds. Fig. 7c and Fig. 7g show the results of background removal and the mapping image (T_{n2}) generated by EBR without denoising, respectively, where $B = 64$, $\hat{M} = 5$, $\hat{N} = 5$, $\tau = 0.4$, $K = 3$, $W_x = 1$, $W_y = 1$, and $\lambda = 5$. Before the execution of the proposed method, Birds was processed through 5×5 Gaussian filtering with a standard deviation of 1.0 and Sobel edge detection. EBR was then executed with $\alpha_f = 0.01$ and $\alpha_h = 0.2$ for denoising. The execution time was 1.07 s. Fig. 7d and 7h show the results and mapping image (T_{e2}), respectively. As shown in Fig. 7g and 7h, most pixels in background could be removed by EBR except the pixels in the regions where the brightness changes drastically. $MSE(T_{h2}, T_{g2})$, $MSE(T_{n2}, T_{g2})$, and $MSE(T_{e2}, T_{g2})$ were 0.419, 0.254, and 0.013, respectively. Therefore, EBR could remove the background of Birds, with a small error rate of 1.3%.

Fig. 8 shows the process of applying EBR to Birds. Fig. 8a, 8b, 8c show $\hat{L}^3$, $\hat{L}^2$, and $\hat{L}^1$, respectively. Fig. 8d, 8e, and 8f show the mapping images without denoising: T^3, T^2, and T^1, respectively. Because the texture of the background of Birds is more complicated than that of Girl, many background pixels could not be removed in T^3. However, the en-

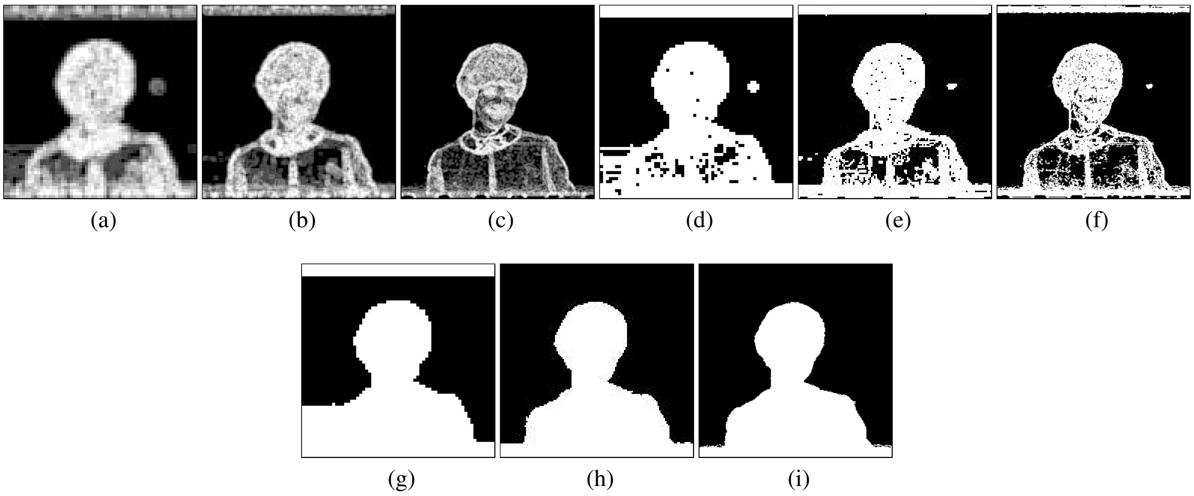

Figure 6: Classification results at each level for Girl. (a),(b),(c) Images filtered by the normalized entropy filter. (d),(e),(f) Mapping images without denoising. (g),(h),(i) Mapping images with denoising. (a),(d),(g) $k = 3$. (b),(e),(h) $k = 2$. (c),(f),(i) $k = 1$.

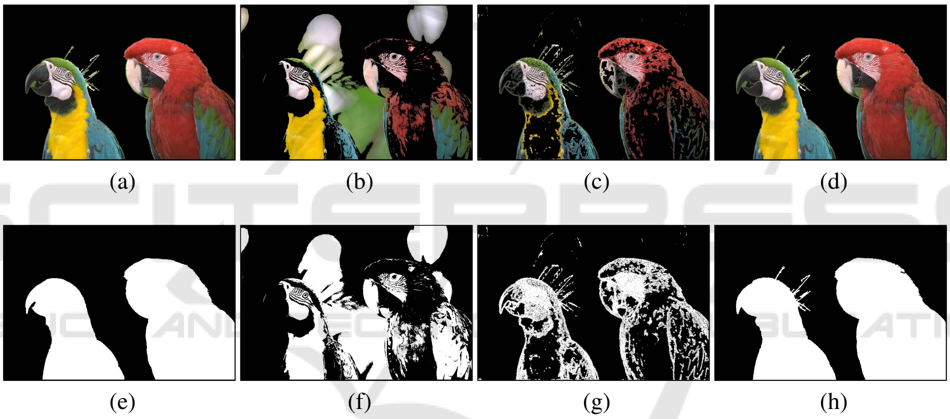

Figure 7: Results of Birds. (a) Ground truth. (b) Result of HB. (c) Result of EBR without denoising. (d) Result of EBR with denoising. (e),(f),(g),(h) Mapping images of (a),(b),(c),(d), respectively.

tropies of most background pixels were lower than the entropies of the pixels in the outlines and textures of the two parrots. Numerous background pixels could be removed in T^1 so that only the outlines and textures of the two parrots were retained. Therefore, applying EBR with denoising could complete the bodies of the parrots, as shown in shown in Fig. 8g, 8h, and 8i ($\bar{T}^3$, $\bar{T}^2$, and $\bar{T}^1$), respectively.

The third test image was Lighthouse, which is a colorful landscape photograph of size 512 × 768 pixels. Fig. 9 shows the test results. This test demonstrated that EBR can remove the background from a landscape photograph if the texture complexities of the background and foreground are different. In Lighthouse, only the pixels in the sky area belong to the background; the other pixels belong to the foreground. Fig. 9a and 9d are the results of manual background removal and the mapping image (T_{g3}), respectively. The result and mapping image (T_{h3}) generated by the HB method are shown in Fig. 7b and Fig. 9e, respectively. The HB method classified the pixels with high intensity as foreground; however, many background pixels with high intensity were also classified as foreground. Fig. 9c and 9f present the result and mapping image (T_{e3}), respectively, generated by EBR with denoising, where $B = 32$, $\hat{M} = 5$, $\hat{N} = 5$, $\tau = 0.3$, $K = 3$, $W_x = 1$, $W_y = 1$, $\lambda = 5$, $\alpha_f = 0.05$, and $\alpha_h = 0.1$. The 5×5 Gaussian filtering with a standard deviation of 1.0 and Sobel edge detection were also applied before the execution of the proposed method. The execution time was 1.09 s. $MSE(T_{h3}, T_{g3})$ and $MSE(T_{e3}, T_{g3})$ were 0.501 and 0.004, respectively. Therefore, EBR removed the background of Lighthouse with an error rate of 0.4%.

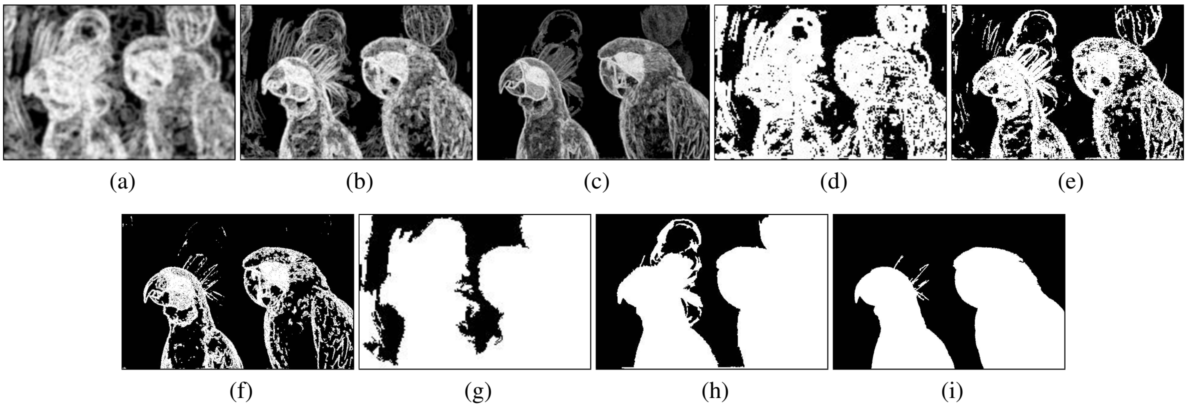

Figure 8: Classification results at each level for Birds. (a),(b),(c) Images filtered by the normalized entropy filter. (d),(e),(f) Mapping images without denoising. (g),(h),(i) Mapping images with denoising. (a),(d),(g) $k = 3$. (b),(e),(h) $k = 2$. (c),(f),(i) $k = 1$.

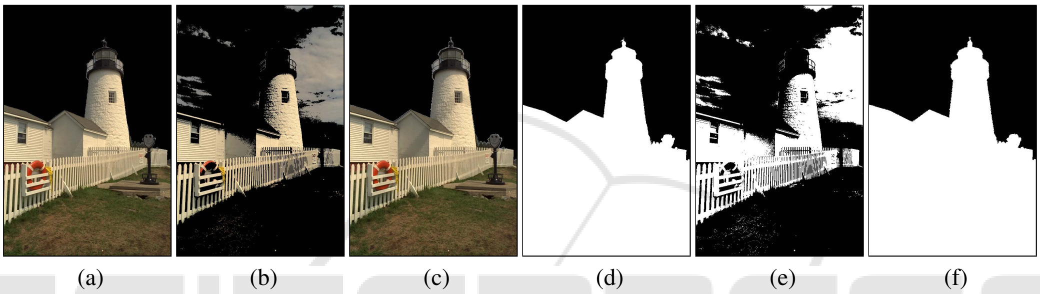

Figure 9: Results of Lighthouse. (a) Ground truth. (b) Result of HB method. (c) Result of EBR with denoising. (d),(e),(f) Mapping images of (a),(b,)(c), respectively.

4 CONCLUSION

This paper presents a method of background removal for a single image. The proposed method uses normalized entropy filtering to compute the texture complexities of the foreground and background. The background can be successfully removed if the entropy distributions of the foreground and background have little overlap.

The proposed method constructs a pyramid to accelerate the computation because substantial background area can be detected in the top level of the pyramid and the entropy computing of this detected background can be ignored in other levels. Many noise areas, including fragments and holes, can be reduced through CCL in the top level to minimize the computing of CCL in the other levels.

Graphical processing unit (GPU) implementation is a topic for future work. The proposed method consists of three main procedures: pyramid construction, normalized entropy filtering, and CCL. These procedures are appropriate for GPU implementation; the performance of the proposed method can reach real-time performance.

The proposed method requires that the textures of foreground and background be different. An ideal case is the first test image, Girl, which has no overlap between the entropy ranges of the foreground and background. In other cases, the proposed method may fail. To address this problem, a clustering method, such as color- or geometry-based clustering, can be applied to the original image such that the foreground can be approximately segmented. The proposed method then can subtly remove the background. Parameter selection is another challenger with the proposed method. Although the parameters of the proposed method can be easily decided if the image was photographed using a shallow depth of field, creating general guidelines to decide the parameters is difficult. This problem can be addressed by a machine learning model or artificial neural network to find an optimal set of parameters automatically.

In summary, the proposed method of background removal is efficient for an image if its foreground and background have different texture complexities. The experimental results demonstrate that the proposed method can successfully remove background pixels with low entropy and retain foreground pixels with high entropy. The results also demonstrate that the computation time of the proposed method is reasonable. An image of 768 × 512 pixels can be processed in approximately 1 s without any parallel computing for acceleration.

ACKNOWLEDGMENTS

This work was sponsored by the Ministry of Science and Technology, Taiwan (109-2221-E-009-142-).

REFERENCES

Adelson, E., Anderson, C., Bergen, J., Burt, P., and Ogden, J. (1983). Pyramid methods in image processing. *RCA Eng.*, 29.

Chen, T., Zhu, Z., Hu, S.-M., Cohen-Or, D., and Shamir, A. (2016). Extracting 3d objects from photographs using 3-sweep. *Communications of the ACM*, 59:121–129.

Gonzalez, R. and Woods, R. (2006). *Digital Image Processing (3rd Edition)*. Prentice-Hall, Inc.

Gordon, G., Darrell, T., Harville, M., and Woodfill, J. (1999). Background estimation and removal based on range and color. In *Proceedings. 1999 IEEE Computer Society Conference on Computer Vision and Pattern Recognition (Cat. No PR00149)*, volume 2, pages 459–464 Vol. 2.

He, L., Chao, Y., Suzuki, K., and Wu, K. (2009). Fast connected-component labeling. *Pattern Recognition*, 42:1977–1987.

He, L., Ren, X., Gao, Q., Zhao, X., Yao, B., and Chao, Y. (2017). The connected-component labeling problem: A review of state-of-the-art algorithms. *Pattern Recognition*, 70.

Huang, Z.-K. and Liu, D.-H. (2007). Segmentation of color image using em algorithm in hsv color space. In *2007 International Conference on Information Acquisition*, pages 316–319.

Junqing Chen, Pappas, T. N., Mojsilovic, A., and Rogowitz, B. E. (2005). Adaptive perceptual color-texture image segmentation. *IEEE Transactions on Image Processing*, 14(10):1524–1536.

Knuth, K. (2006). Optimal data-based binning for histograms. *arXiv*.

Kodak. The kodak image dataset.

Kumar, S. and Yadav, J. (2016). Video object extraction and its tracking using background subtraction in complex environments. *Perspectives in Science*, 8.

Malik, J., Belongie, S., Leung, T., and Shi, J. (2001). Contour and texture analysis for image segmentation. *International Journal of Computer Vision*, 43:7–27.

Purwani, S., Supian, S., and Twining, C. (2017). Analyzing the effect of bin-width on the computed entropy. *Journal of Informatics and Mathematical Sciences*, 9(4).

Qi, C. (2014). Maximum entropy for image segmentation based on an adaptive particle swarm optimization. *Applied Mathematics & Information Sciences*, 8:3129–3135.

Ronneberger, O., Fischer, P., and Brox, T. (2015). U-net: Convolutional networks for biomedical image segmentation. In *Medical Image Computing and Computer-Assisted Intervention – MICCAI 2015*, pages 234–241. Springer International Publishing.

Schroff, F., Criminisi, A., and Zisserman, A. (2008). Object class segmentation using random forests. In *Proceedings of the British Machine Vision Conference*, pages 54.1–54.10. BMVA Press.

Shannon, C. E. (2001). A mathematical theory of communication. *SIGMOBILE Mob. Comput. Commun. Rev.*, 5(1):3–55.

Soman, J., Kothapalli, K., and Narayanan, P. (2010). Some gpu algorithms for graph connected components and spanning tree. *Parallel Processing Letters*, 20:325–339.

Tsai, Y.-P., Ko, C.-H., Hung, Y.-P., and Shih, Z.-C. (2007). Background removal of multiview images by learning shape priors. *IEEE transactions on image processing : a publication of the IEEE Signal Processing Society*, 16:2607–16.

USC-SIPI. The usc-sipi image database.

Wang, x. y., Wang, T., and Bu, J. (2011). Color image segmentation using pixel wise support vector machine classification. *Pattern Recognition*, 44:777–787.

Zhang, H., Fritts, J. E., and Goldman, S. A. (2003). An entropy-based objective evaluation method for image segmentation. In *Storage and Retrieval Methods and Applications for Multimedia*.

Zhang, Y. and Luo, L. (2012). Background extraction algorithm based on k-means clustering algorithm and histogram analysis. volume 2, pages 66–69.